Rapid Simulation of Scattering Parameters for Coupled Waveguides with Arbitrary Geometries

Easton Potokar, *Student Member, IEEE,* R. Scott Collings, *Student Member, IEEE,* Alec M. Hammond, *Student Member, IEEE,* Ryan M. Camacho, *Member, IEEE*

Abstract—We present a new method to accurately simulate arbitrarily shaped coupled waveguides and ring resonators 100 to 1000 times faster than existing techniques. The new method uses a novel analytic formulation and multivariate polynomial regression to map the physical dimensions of the simulated waveguides to the complex cross-coupling coefficients of input and output ports, giving the full scattering parameters. We benchmark the results against full-wave solutions and illustrate its use with several application examples.

I. Introduction

Waveguide coupling is one of the backbones of future photonic integrated circuits. Many devices leverage coupling for power-splitting, filtering, wavelength-selective dropping, etc [1] [2]. However, simulation of these devices using full-wave methods such as finite-difference time domain (FDTD) is computationally expensive.

Several compact models have been proposed to avoid full-wave methods and simulate complex photonic structures. Power splitting in directional couplers, for example, has been designed through asymmetric-waveguide phase control sections [1]. Other methods based on the transfer matrix method vary the shape of geometry to arrive at desired power splitting ratios [3]. Some directional coupler models discretize the coupler into multiple uniform coupling regions and approximate the effective indices of each region using exponential regression [4]. Previous implementations of the this method have been demonstrated for specific devices such as half ring and racetrack resonators, but are not implemented for directional couplers with arbitrary geometries such as irregularly shaped power splitting devices. They also have an additional limitation of only tracking magnitude, but not the phase, of the output fields thereby restricting the ability to generate full scattering parameters.

To overcome these limitations, we propose a new model, which we name SCEE (simulator of photonic coupling devices based on eigenmode estimation). SCEE extends a recent model proposed by M Bahadori et al. [4], adding phase correction terms, leveraging multivariate linear regressions, and implementing numerical quadratures techniques. This allows simulation of scattering parameters (amplitude and phase) of coupling devices with arbitrary geometries. With full scattering parameters, arbitrary coupling devices can be concatenated with any other devices in full photonic circuits. When compared to Lumerical's full-wave 2.5D varFDTD, SCEE performs an order of magnitude faster for 20 μm devices and nearly 2 orders of magnitude faster for 40 μm

devices. Furthermore, since SCEE relies entirely on the speed at which the scale-invariant numerical quadratures are computed, and is thus also scale invariant. SCEE can therefore handle devices of arbitrarily large dimensions.

These improvements enable the design of novel devices such as ring resonators with multiple coupling regions and unitary transformers using cascaded devices. Furthermore, other devices that require hours of simulation time using full-wave methods can now be simulated in seconds. Additionally, because SCEE performs much faster than full-wave methods, researchers can employ advanced forward and inverse design techniques, as demonstrated below, through optimization.

The rest of the paper is outlined as follows: in section II, we briefly review the model proposed by Bahadori et al. [4]. In section III we give an outline of extensions to the model that enable accurate phase retrieval and arbitrary waveguide geometries and paths. In section IV we discuss the results of SCEE compared to full-wave methods in both speed and accuracy. Section V shows how SCEE can be used to design custom power splitters, ring-resonators with multiple coupling regions, and unitary transformers using cascaded devices.

II. Modeling of Directional Coupler

In this section, we review the essential features of a recently proposed compact model [4] for simulating the full scattering parameters of directional couplers. In section III, we show how this model can be extended to include phase scattering terms and arbitrary geometries.

In nearly all integrated photonic couplers, there exists a sub-wavelength region in which the gap between waveguides is small and optical coupling takes place. By discretizing this region and parameterizing it by a nonuniform gap distance between the two coupling waveguides, each discrete section may be assumed to be a directional coupler with uniform gap distance as shown in Fig. 1(a). Each of these sections may be described by a transfer matrix of the form

$$T_i = \begin{bmatrix} t_i & \kappa_i \\ \kappa_i & t_i \end{bmatrix} = \exp(-j\phi_i) \begin{bmatrix} |t_i| & -j|\kappa_i| \\ -j|\kappa_i| & |t_i| \end{bmatrix}, \quad (1)$$
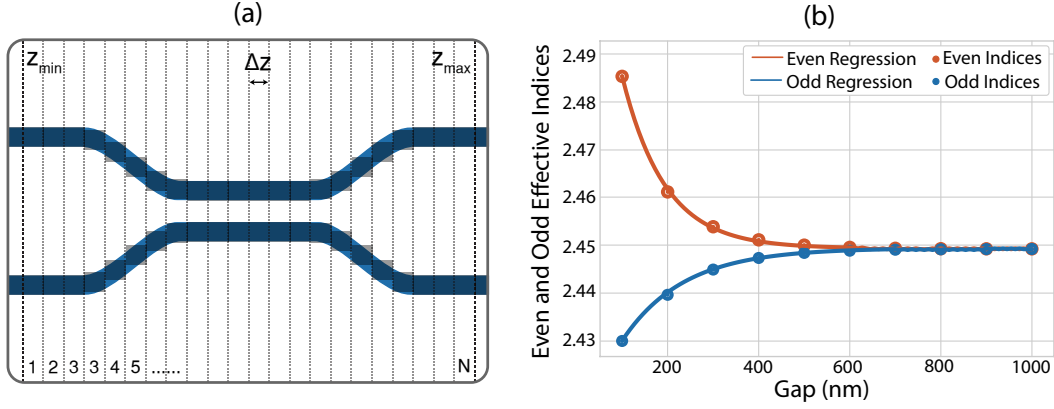
where

Fig. 1. (a) Schematic for splitting directional coupler of length $z_{max} - z_{min}$ into N discrete uniform couplers each with length Δz. (b) Exponential regression of even and odd supermodes.

$$\phi_i = \frac{2\pi}{\lambda} \Delta z \frac{n_{\text{even}}[g_i] + n_{\text{odd}}[g_i]}{2}, \tag{2a}$$

$$|t_i| = \cos\left(\frac{2\pi}{\lambda} \Delta z \frac{n_{\text{even}}[g_i] - n_{\text{odd}}[g_i]}{2}\right), \tag{2b}$$

$$|\kappa_i| = \sin\left(\frac{2\pi}{\lambda} \Delta z \frac{n_{\text{even}}[g_i] - n_{\text{odd}}[g_i]}{2}\right). \tag{2c}$$

In Eqns. (1)-(2c), g_i is the uniform gap distance between waveguide edges, t represents the scattering parameters out of the through-port, κ the scattering parameters out of the cross-port, λ the wavelength, Δz the length of the discretized section, and $n_{\text{even}}[g_i]$ and $n_{\text{odd}}[g_i]$ the effective indices of the even and odd supermodes as a function of gap distance. $n_{\text{even}}[g_i]$ and $n_{\text{odd}}[g_i]$ are fitted with an exponential regression as shown in Fig. 1(b) and are estimated as a function of gap g with equations

$$n_E \approx n_{\text{eff}} + a_E \exp(-\gamma_E\, g), \tag{3a}$$

$$n_O \approx n_{\text{eff}} - a_O \exp(-\gamma_O g). \tag{3b}$$

As shown graphically by M. Bahadori et al. [4], this approximation holds well for $g > 100$ nm, but underestimates the coupling by 5-10% when $g < 100$ nm, especially in regions of large curvature.

The transfer matrix T of the entire coupling region is found by cascading the transfer matrices of the discrete regions, $T = T_N \times T_{N-1} \times \cdots \times T_2 \times T_1$. This final transfer matrix can be rewritten as

$$T = \exp(-j\phi_+)\begin{bmatrix} \cos(\phi_-) & -j\sin(\phi_-) \\ -j\sin(\phi_-) & \cos(\phi_-) \end{bmatrix} \tag{4}$$

where

$$\phi_+ = \frac{2\pi}{\lambda} \sum_{i=1}^{N} \frac{n_{\text{even}}[g_i] + n_{\text{odd}}[g_i]}{2} \Delta z, \tag{5a}$$

$$\phi_- = \frac{2\pi}{\lambda} \sum_{i=1}^{N} \frac{n_{\text{even}}[g_i] - n_{\text{odd}}[g_i]}{2} \Delta z. \tag{5b}$$

Thus, the coupling coefficients, t and κ, corresponding to the through-port and cross-port may be computed using Eqns.

(4), i.e. $t = e^{-j\phi_+}\cos(\phi_-)$ and $\kappa = -je^{-j\phi_+}\sin(\phi_-)$. Further details of this derivation can be found in [4].

As the number of discrete coupling regions $N \to \infty$, $\Delta z \to 0$, Eqns. (5a) and (5b) become integrals. Using the exponential regressions mentioned in Eqns. (3a) and (3b) the magnitude of the coupling coefficients may be expressed as

$$|\kappa| = \sin\left(\frac{\pi}{\lambda} \int_{z_{min}}^{z_{max}} a_E e^{-\gamma_E g(z)} + a_O e^{-\gamma_O g(z)} dz\right), \tag{6a}$$

$$|t| = \cos\left(\frac{\pi}{\lambda} \int_{z_{min}}^{z_{max}} a_E e^{-\gamma_E g(z)} + a_O e^{-\gamma_O g(z)} dz\right). \tag{6b}$$

where $g(z)$ gives the gap distance between the waveguides for the corresponding value of z along the coupling region.

While this model accurately describes the amplitude of the transmitted and coupled light waves, it has two major limitations. The first is that it does not accurately predict the resulting phase terms of the coupled light associated with the amplitudes $|\kappa|$ and $|t|$. The phase is a critical parameter for building resonant devices and cascading multiple devices to form complete photonic circuits. The second limitation is that it does not allow for arbitrary waveguide geometries and paths. In section III, we extend this model to include both of these features.

III. MODEL EXTENSIONS

A. Phase Correction Terms

We begin by showing how to extend the model described above to include an accurate calculation of the phase of the transmitted and coupled light waves. Similar to the derivation of the field magnitude Eqns. (6a) and (6b), we find the phase by taking the limit in which the number of discrete coupling regions $N \to \infty$, $\Delta z \to 0$, which makes Eqns. (5a) and (5b) integrals. By examining the ϕ_+ term and substituting in the
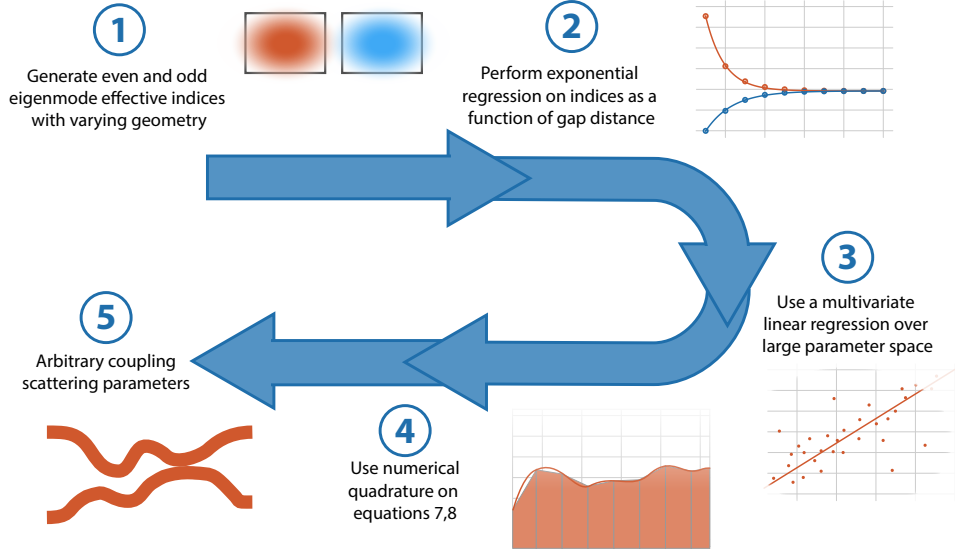
Fig. 2. SCEE overview. First even and odd eigenmode effective indices were generated for various waveguide gaps with fixed geometry (1). An exponential regression was fit to get parameters a_E, γ_E, a_O, and γ_O (2). Next a polynomial regression maps waveguide properties (wavelength, width, thickness) to parameters a_E, γ_E, a_O, and γ_O (3). Then to calculate s-parameters a numerical quadrature is done using eqns 6 and 8 (4). The s-parameters are then used to calculate the coupling of arbitrary directional couplers (5).

exponential regressions found in Eqns. (3a) and (3b), we arrive at

$$\angle \kappa = \exp\left(-j\left(\frac{\pi}{\lambda} \int_{z_{min}}^{z_{max}} a_E e^{-\gamma_E g(z)} - a_O e^{-\gamma_O g(z)} dz \right.\right.$$
$$\left.\left. + \frac{2\pi}{\lambda} \int_{z_{min}}^{z_{max}} n_{\text{eff}} dz + \frac{\pi}{2} \right) \right), \quad (7a)$$

$$\angle t = \exp\left(-j\left(\frac{\pi}{\lambda} \int_{z_{min}}^{z_{max}} a_E e^{-\gamma_E g(z)} - a_O e^{-\gamma_O g(z)} dz \right.\right.$$
$$\left.\left. + \frac{2\pi}{\lambda} \int_{z_{min}}^{z_{max}} n_{\text{eff}} dz \right) \right) \quad (7b)$$

Note that the last term in Eqns. (7a) and (7b) is the phase change of a straight waveguide of length $z_{max} - z_{min}$. This is a result of the assumption that our waveguide is made up of uniform couplings. To remove the dependence on this assumption, we modify the integrals to instead integrate over the arc length of waveguides with potentially arbitrary paths. Letting z_c represent the value of z corresponding to location of the minimum gap distance, we arrive at Eqns. (8a) and (8b), where $t(z)$ and $\kappa(z)$ are the geometries of the through and cross waveguides, respectively. Physically, for the through port this represents the entire arc length of the through waveguide,

and for the cross port, it represents the sum of the through waveguide arc length up to z_c and cross waveguide arc length after z_c. Note for the case of the symmetric coupler, (i.e. both the cross and through waveguides are identical) these equations simplify since $\kappa(z) = t(z) = \frac{g(z)}{2}$.

B. Leveraging Regression to fit Arbitrary Geometries

Given a waveguide geometry with a gap function $g(z)$ defining the gap throughout the coupling region, the effective index estimation coefficients, a_E, γ_E, a_O, and γ_O, from Eqns. (3a), (3b) must be found to perform the integrations (6a), (6b), (8a), ant (8b) that calculate κ and t. These coefficients will be dependent on the wavelength, width, and thickness of the waveguide. To estimate these coefficients for all such combinations we performed a multivariate polynomial regression on many different waveguide geometries. First we generate data to gather these coefficients by running simulations using a modified version of the finite difference eigenmode solver WGMS3D [5], a 3D waveguide modesolver, with a custom python wrapper pyMode [6]. To get effective index estimation coefficients for a fixed geometry, an exponential regression was run on simulations of two symmetric SiO$_2$-cladded Si waveguides with the gap distance varying between 100 and 1000 nm as seen in Fig. 1(b). This was repeated for over 7000

$$\angle \kappa = \exp\left(-j\left(\frac{\pi}{\lambda} \int_{z_{min}}^{z_{max}} a_E e^{-\gamma_E g(z)} - a_O e^{-\gamma_O g(z)} dz + \frac{2\pi}{\lambda} n_{\text{eff}} \left(\int_{z_{min}}^{z_c} \sqrt{1 + t'(z)} dz + \int_{z_c}^{z_{max}} \sqrt{1 + \kappa'(z)} dz \right) + \frac{\pi}{2} \right) \right),$$
$$(8a)$$

$$\angle t = \exp\left(-j\left(\frac{\pi}{\lambda} \int_{z_{min}}^{z_{max}} a_E e^{-\gamma_E g(z)} - a_O e^{-\gamma_O g(z)} dz + \frac{2\pi}{\lambda} n_{\text{eff}} \int_{z_{min}}^{z_{max}} \sqrt{1 + t'(z)} dz \right) \right),$$
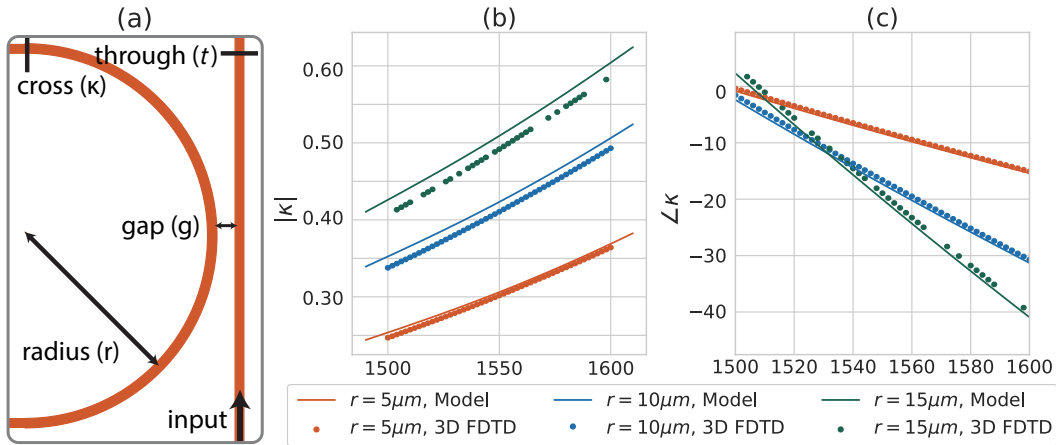$$(8b)$$

Fig. 3. (a) Diagram of half ring resonator. (b) Magnitude and (c) phase results for a Half Ring Resonator with closest gap distance of 100 nm. Waveguide geometry is 450 nm width and 220 nm thickness. Plots are shown as a function of wavelength for 3 different radii, 5, 10, and 15 μm.

different waveguide geometries varying wavelength from 1450 nm to 1650 nm, width from 400 nm to 600 nm, thickness from 180 nm to 240 nm, and sidewall angles from 80 to 90 degrees. In combination with the range of gaps, this resulted in over 75,000 simulations. The simulations were performed using BYU's supercomputer, with 1000 jobs running in parallel. Each job used a single 2.3GHz core with 20GB of memory, and took 5.5-8 hours to complete.

In addition, a multivariate polynomial regression was performed that maps thickness, width, wavelength, and sidewall angle to the effective index estimation coefficients. In this way, the effective index estimation coefficients may be found for any wavelength, thickness, width, and wavelength. Furthermore, we can accurately predict parameters outside the original dataset to find a continuous set of effective index estimation coefficients. The regression was trained using the python package sklearn [7] resulting in a mean-square-error (MSE) less than 10^{-5}, which shows SCEE provides exceptionally accurate estimates.

IV. SCEE VS. FDTD SIMULATIONS

A. SCEE Accuracy

To verify the results of the multivariate regression, 3D FDTD simulations of half ring couplers as shown in Fig. 3(a) were run using meep [8], an open-source FDTD solver. These half ring couplers have waveguide geometries of width 450 nm, thickness 220 nm, and radii of 5, 10 and 15 microns. The closest coupling gap was 100 nm for each radius.

Our predictions of κ and t were found using Eqns. (6a), (6b), (8a), (8b) along with the multivariate regression and SciPy's quadrature routines[9] (to estimate the integrals) described above. The results of the FDTD simulations and our predictions are shown in Figs. 3(b) and 3(c). There is good agreement between the two, with small errors in both magnitude and phase.

B. SCEE Speed

To verify that SCEE also yields speed improvements over full-wave techniques, we compared it to Lumerical's varFDTD
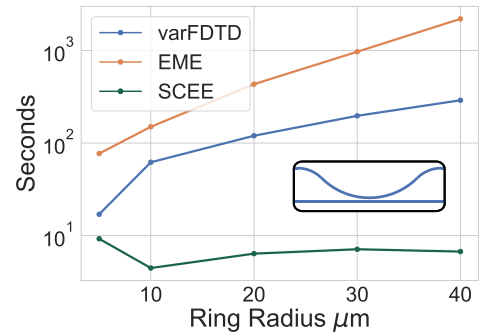

Fig. 4. Speed comparisons of SCEE , Lumerical's varFDTD and Lumerical's EME simulations for shown device with varying radii.

and EME methods. We simulated part of a ring resonator with rings ranging from 5 μm to 40 μm and s-bends to straighten the end of the waveguides. varFDTD simulations were run with a non-uniform mesh setting of 4 to balance speed and accuracy. The EME simulations were run with transverse mesh settings ranging from 0.05 μm to 0.1 μm based on the location, and a cell placed every 0.2 μm. SCEE was timed simulating an identical model. The results and device are shown in Fig. 4, demonstrating that SCEE performed 1 order of magnitude faster for 20 μm devices and nearly 2 orders of magnitude faster for 40 μm devices.

We note that SciPy's quadrature calculation routines are known to have temporal complexity no worse than $O(N)$, where N is the number of integrand evaluations. Since SCEE relies entirely on the speed at which the quadrature is computed, it is scale invariant; meaning that even as devices get larger, the number of integrand evaluations does not increase. This can be seen in Fig. 4 as the total time of simulation is approximately constant for SCEE as the radii increases. This is in contrast to full-wave techniques, for which the simulation times scales exponentially with model size.

SciPy's quadrature calculation routines are adaptive, meaning they will detect how many integrand evaluations N are needed for accurate results. Interestingly, due to the smaller
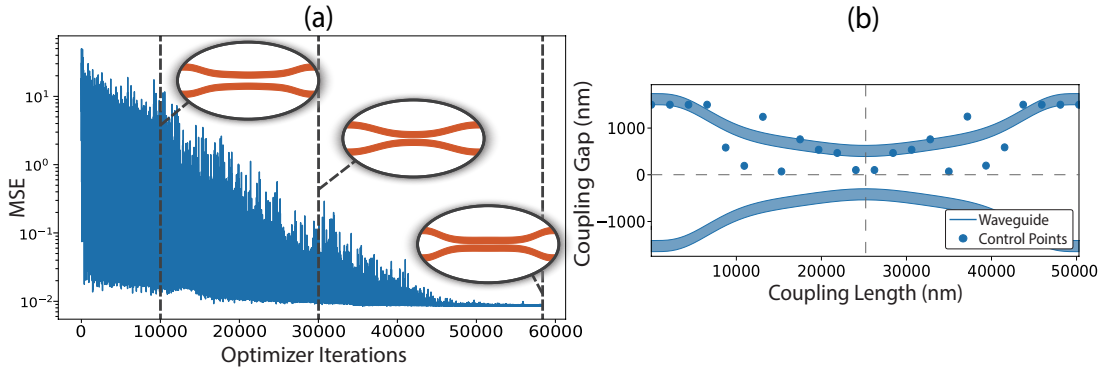
Fig. 5. (a) MSE for desired power splitting ratio as a function of optimizer iterations. Shows the evolution of coupler at iterations 10,000, 30,000, and 58,000 (b) Example of how control points were used to determine gap distance and thus waveguide geometry at each iteration of optimizing the directional coupler.

average spacing between waveguides g in the in the smallest device simulated (5μm radius), the exponential terms in Eq. 6 are larger, and hence discretized more finely by the adaptive routine, thus resulting in a *greater* simulation time when compared to larger devices. This is clearly seen in Fig. 4, in which the smallest device has the longest simulation time using SCEE .

V. APPLICATIONS

To demonstrate SCEE's utility, we describe three devices simulated using SCEE that are (1) intractable to simulate using traditional full-wave techniques, and (2) cannot be accurately simulated with existing compact models. We first describe the inverse design of directional couplers with arbitrary waveguide geometries. We next describe a ring resonator coupled to a single waveguide with two distinct coupling regions. Finally, we describe a complex circuit consisting of >20 individual directional couplers cascaded to form a unitary transformer.

A. Accelerated Inverse Design of Custom Power Splitters

Due to the speed of SCEE , we can effectively solve inverse design problems. To illustrate this capability, we use SCEE to design a directional coupler with a desired power ratio from cross-port to through-port. Here we assume that the input magnitude is unity so we only need to specify $|\kappa_{goal}|^2$ for the ratio ($|t|^2 = 1 - |\kappa|^2$). A different choice for the input magnitude would simply create a scaling factor for the outputs $|\kappa|^2$ and $|t|^2$. We create an inverse design optimizer that takes as an input $|\kappa_{goal}|^2$ and outputs a directional coupler geometry that produces the desired coupling ratio. The coupler is parameterized by coupling length, $z_{max} - z_{min}$, and 16 discrete points, spaced evenly along the coupling length, that define the gap between the two waveguides in terms of a bezier curve (described below). This allows the optimizer to easily manipulate the design of the coupler with fewer degrees of freedom. The objective function of the optimizer is the mean-square error (MSE) for four distinct wavelengths evenly spaced between 1500-1600 nm of the power equation $-10 \log_{10} |\kappa|^2/|\kappa_{goal}|^2$. For each iteration $|\kappa|^2$ is calculated at the four wavelengths using SCEE . Figure 5(a) illustrates the evolution of the optimizer through approximately 58,000

complete simulations of a full directional coupler in less than 60 minutes. This large number of iterations is only feasible since SCEE computes each iteration much faster than traditional solvers.

The waveguides in this example were chosen to be 220 nm in thickness and 450 nm in width, although SCEE accepts arbitrary width and thickness geometries. The optimizer uses the nlopt python package[10] to perform the optimization, first performing a bounded global optimization using the ISRES routine with bounds of 0 to 1500 nm for the gap function's control points, then performing a local optimization using the SLSQP routine on the results of the global optimization. Among the various routines tested, these are the only ones that both accepted the constraints detailed below and gave consistently good results. We refer the reader to the nlopt documentation for further details on the algorithms.

While we optimize over the control points of a gap function $g(z)$, the designed waveguide does not necessarily pass through these control points. Rather, the control points define $g(z)$ using the Bernstein transformation

$$g(z) = \hat{g}\left(\frac{z}{z_{max} - z_{min}}\right) = \hat{g}(t) = \sum_{i=0}^{n} g_i B_{i,n}(t), \quad (9)$$

with t ranging from 0 to 1, where each g_i is the gap value of the ith control point, spaced evenly along the coupling length and $B_{i,n}(t) = \binom{n}{i} t^i (1-t)^{n-i}$ are the Bernstein polynomials. Figure 5(b) shows the waveguide geometry and corresponding control points for one iteration of the optimizer.

In order to produce physically realizable devices, several constraints were imposed on $\hat{g}(t)$. First, we required that $\hat{g}(t) \geq 100$ nm for every t, to ensure that the exponential regressions in Eqns. (3a) and (3b) remain valid. This is accomplished by imposing a penalty on any iteration of $\hat{g}(t)$ that violates this constraint. Second, we require that $\hat{g}(0) = \hat{g}(1) = 1500$ nm, thus ensuring that no coupling occurs at the inputs or outputs. For simulation convenience, we also impose several symmetries. We impose symmetry such that $\hat{g}(t) = \hat{g}(1-t)$, thus creating a waveguide that is symmetric across the coupling length. The optimized directional coupler also has waveguides that are mirror images of each other, thus the $g(z)$ is twice the distance from each waveguide to the center line. These symmetries are illustrated by the
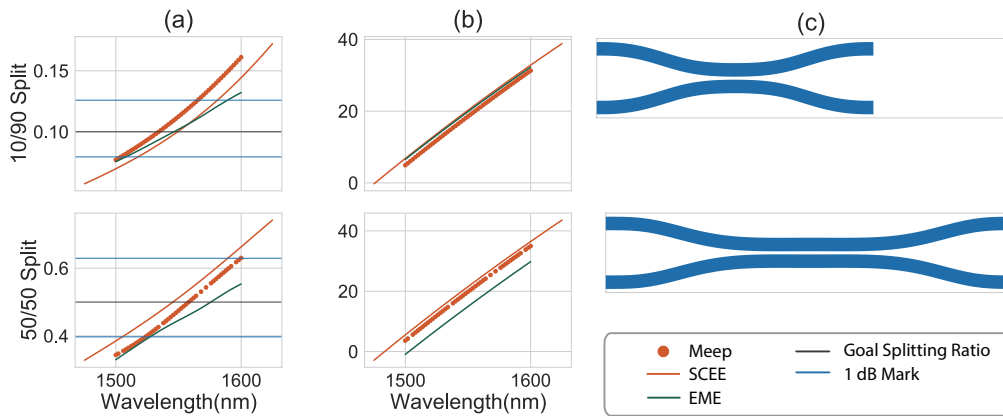
Fig. 6. Comparison of output from SCEE vs FDTD for couplers optimized for $|\kappa_{goal}|^2 = 0.10$ and $|\kappa_{goal}|^2 = 0.50$. Shown is (a) $|\kappa|^2$, (b) $\angle\kappa$ in radians, and (c) the resulting waveguide geometries with lengths 9 μm and 13 μm respectively.

vertical and horizontal dashed lines respectively in Fig. 5(b). Finally, we impose a constraint on the waveguide curvature to prevent bending loss. Specifically, we require that the radius of curvature at any point along the waveguide is at least five microns, or $|K(t)| \leq 1/5 \ \mu\text{m}^{-1}$.

Using this inverse design optimizer for directional couplers, we found that any $|\kappa_{goal}|^2$ between 0.08 and 0.50 can be obtained within 1.5 dB for wavelengths between 1500-1600 nm. In all cases, $|\kappa|^2$ is within 1 dB of $|\kappa_{goal}|^2$ across at least two-thirds of the target wavelength spectrum of 1500-1600 nm. For an even smaller target coupling ratio of $|\kappa_{goal}|^2 = 0.01$, the optimizer finds a solution within 2 dB of $|\kappa_{goal}|^2$ for the entire wavelength range, and within 1 dB for 58% percent of the range.

Figure 6 shows that simulations using SCEE and using FDTD (using meep) are in very good agreement for two representative directional couplers optimized to have $|\kappa_{goal}|^2 = 0.50$ and $|\kappa_{goal}|^2 = 0.10$.

A few remarks are useful to compare these results with other emerging inverse design techniques using shape and topology optimization. Shape and topology optimization (TO) typically relies on adjoint variable methods (AVM) that efficiently compute the gradient of the merit function with respect to the degrees of freedom. Adjoint methods are especially important when each optimization iteration is computationally expensive (i.e. an FDTD simulation) and the user specifies several degrees of freedom.

Our method, however, is computationally cheap and benefits from relatively simple parameterizations. While implementing an AVM that backpropagates the gradient through the analytical and regression inference models presented here would be straightforward, SCEE is sufficiently fast to implement classic gradient-free algorithms (both local and global) as described above. Unlike classical TO methodologies, however, we parameterized our example designs using splines and other continuous functions, rather than polygonal points or density voxels.

B. Doubly Coupled Ring Resonators

As a second example, we calculate the output spectrum of a ring resonator which is coupled to a waveguide at two locations as seen in Fig. 7(a). This is a potentially important devices for implementing single-photon nonlinearities, and can be used to improve the performance of quantum devices such as single-photon sources and atom-like quantum memories with photon interfaces [11].

Modeling of the doubly-coupled ring resonator demonstrates two key aspects of SCEE . The first is the ability of SCEE to accurately calculate both the phase and amplitude of light within the simulated devices, and thereby construct the full s-parameters of the device. The second is the ability of SCEE to use the resulting s-parameters to cascade multiple individual components to form a complex structure.

The ring was chosen to have radius 30 μm with waveguides having thickness 220 nm and width 500 nm. The doubly coupled ring resonator was modeled in SCEE as two separate identical coupling regions, divided down middle, as shown by the dashed line in Fig. 7(a). The scattering parameters of each coupling region were calculated using SCEE , then stitched together using a custom photonic toolbox simphony [12]. The resulting spectrum is shown in Fig. 7(b) overlayed with a simulation of an identical structure using Lumerical varFDTD.

As we expect from double-coupled rings, the resonant spectra of a single ring is modulated by an envelope resulting from the interference condition imposed by the the two coupling regions. Accurately modeling this complex interference pattern would be impossible without carefully tracking the phase of the field, demonstrating the power of SCEE . Notably, the free-spectral range of both the resonant peaks and the envelope is captured by SCEE . The magnitude of the envelope function does not match perfectly, which we attribute to different waveguide loss models in the two simulations.

C. Arbitrary Unitary Transformers using Cascaded Devices

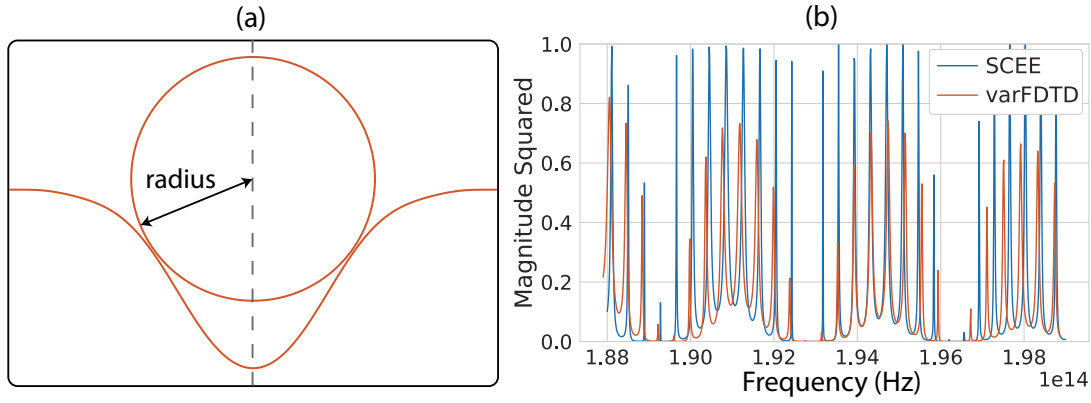As a final application example, we demonstrate the simulation of a complex unitary transformer consisting of tens

(a)

(b)

Fig. 7. (a) Double Coupled Ring with radius 30 μm, waveguide width 500 nm, thickness 220 nm (b) Results from SCEE compared to Lumerical varFDTD simulations for the Double Coupled Ring
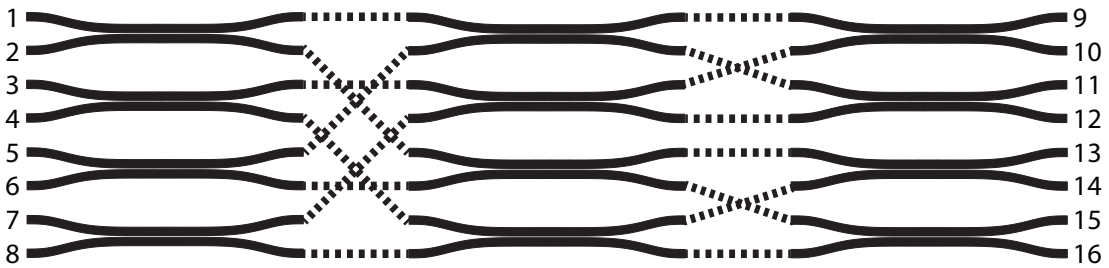

Fig. 8. Cascaded couplers optimized for a 50/50 power split. Dashed lines represent port connections. Output port numbers change after relabeling ports

of individual couplers. The unitary transform we model is shown in Fig. 8, and is known in the literature as a "Green Machine" [13], [14]. This device can be used as a superadditive structured receiver for transmitting information across an optical channel at a rate exceeding the classical Holevo limit. Interestingly, it has yet to be implemented in an integrated photonic structure, though several researchers have made attempts [13]. Here we simulate an 8x8 version of the ideal Green Machine using directional couplers as described in [14]. This Green Machine can be entirely composed of 50/50 directional couplers cascaded together, as shown in Fig. 8. The solid lines represent components designed and simulated using SCEE , and the dashed lines represent connections implemented among these devices using simphony [12].

In this model we assume that the dashed lines are ideal crossings, with complete power transfer and no phase offset. This represents an ideal Green Machine without errors, whereas in non-ideal devices, errors may be introduced by phase and amplitude deviations in the crossings. We include these deviations in further simulations below. As shown above, the 50/50 directional coupler does not split light evenly for all wavelengths, but there is an optimal wavelength at which it does, in this case λ_0 =1546.0842 nm. By injecting light at λ_0 into any of the inputs 1-8, each of the output ports 9-16 will have equal magnitudes but different phases. After relabeling the output ports, the explicit transfer matrix at λ_0 for all combinations of inputs and outputs is given in Eqn. (10). G_3 can be defined recursively as $G_n = \begin{bmatrix} G_{n-1} & iG_{n-1} \\ iG_{n-1} & G_{n-1} \end{bmatrix}$ where $G_0 = \begin{bmatrix} 1 \end{bmatrix}$. Each G_n is a matrix with orthogonal

columns that allows for the creation of unique codewords for a communication channel. Therefore, since the transfer matrix is a constant multiple of $G_3^\dagger$, it also creates unique codewords. If a wavelength other than λ_0 is used, the transfer matrix still has orthogonal columns, but the output port magnitudes will not be equal.

$$\frac{1}{\sqrt{8}}G_3^\dagger = \frac{1}{\sqrt{8}}\begin{bmatrix} 1 & i & i & -1 & i & -1 & -1 & -i \\ i & 1 & -1 & i & -1 & i & -i & -1 \\ i & -1 & 1 & i & -1 & -i & i & -1 \\ -1 & i & i & 1 & -i & -1 & -1 & i \\ i & -1 & -1 & -i & 1 & i & i & -1 \\ -1 & i & -i & -1 & i & 1 & -1 & i \\ -1 & -i & i & -1 & i & -1 & 1 & i \\ -i & -1 & -1 & i & -1 & i & i & 1 \end{bmatrix}^\dagger \tag{10}$$

Moreover, since all possible path lengths from input to output are the same in this scenario for each wavelength, the relative phase of light at the output ports can be written as a matrix [see Eqn. (10)]. The rows represent output ports and columns represent input ports. Each column of this matrix is orthogonal to the other columns, enabling an orthogonal basis for codewords with phase differences of $\pi/2$ radians. Characterization of this device with light input to port 1 is shown in 9(a) as simulated by SCEE .

We next introduced non-ideal crossover elements into the Green Machine simulations in place of the ideal crossovers. This was accomplished by using SCEE and the methods in Section V-A to design a new directional coupler that outputs
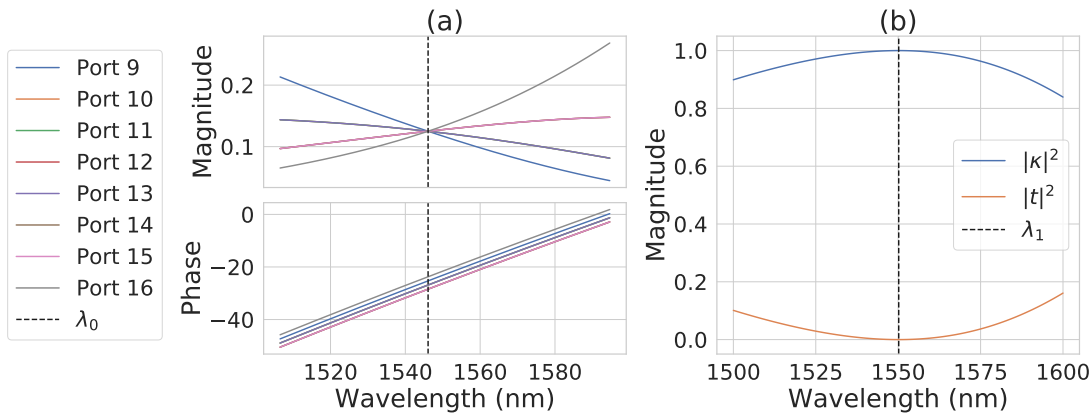
Fig. 9. (a) Output of ideal Green Machine (b) Magnitude output of crossover designed using SCEE and Section V-A

nearly 100% of the light to one of the outputs, and introducing the resulting s-parameters into the the circuit simulation in place of the ideal crossovers. The crossover coupler is such that at the optimal wavelength $\lambda_1 = 1550.1629$ nearly 100% of the light is coupled to the cross port. The transmission vs. wavelength of this coupler is shown in Fig. 9(b).

To preserve the phase relationship among devices, additional waveguide lengths were also introduced to preserve the path lengths at the crossings. The new device also produces a near-ideal matrix at $\lambda_1 = 1550.1629$, though it is rotated owing to a $\pi/2$ phase shift introduced by the 100/0 directional couplers.

Modeling the Green Machine is dependent on having accurate compact models of both a 50/50 directional coupler and a 100/0 directional coupler, both of which are enabled by SCEE 's power to solve inverse design problems. Further, without being able to track the phase of the field, the interactions between each directional coupler in the Green Machine would not be known, again showing the importance that SCEE is able to compute full s-parameters. Finally, due to the large size, traditional FDTD methods would take an intractable amount of time to simulate the Green Machine, while SCEE simulates it in less than a minute per wavelength.

VI. CONCLUSION

By extending the compact model for power splitting proposed by M. Bahadori, et al [4], we have created a new compact model that can simulate waveguides of any width, thickness, and sidewall angle at at any wavelength. Further, this model, SCEE , can handle arbitrary coupling geometries allowing many new devices to be simulated. In addition, SCEE also calculates the complete scattering parameters allowing simulated devices to be stitched to form complex photonic circuits composed of many elements.

These results show that SCEE can be used to accurately and quickly simulate a wide variety of coupling devices. SCEE is scale invariant and is orders of magnitude faster than traditional full-wave methods. Thus devices can be simulated with sufficient accuracy for quick design turnaround and SCEE enables many new possible design tools due to it's speed, including inverse design. SCEE may also enable new accelerated

Monte Carlo methods for uncertainty quantification, which is important for integrated photonic circuit design.

As illustrative examples, we have presented several applications using SCEE including power splitters, doubly coupled ring resonators and a complex unitary transformer. SCEE is open source and is available on github via the SiPANN repository [15].

REFERENCES

[1] Z. Lu, H. Yun, Y. Wang, Z. Chen, F. Zhang, N. A. F. Jaeger, and L. Chrostowski, "Broadband silicon photonic directional coupler using asymmetric-waveguide based phase control," *Opt. Express*, vol. 23, no. 3, pp. 3795–3808, Feb 2015. [Online]. Available: http://www.opticsexpress.org/abstract.cfm?URI=oe-23-3-3795

[2] L. Chrostowski and M. Hochberg, *Silicon photonics design: from devices to systems*. Cambridge University Press; Cambridge, United Kingdom, 2016.

[3] G. F. R. Chen, J. R. Ong, T. Y. L. Ang, S. T. Lim, C. E. Png, and D. T. H. Tan, "Broadband silicon-on-insulator directional couplers using a combination of straight and curved waveguide sections," *Scientific Reports*, vol. 7, no. 1, pp. 2–5, Aug. 2017. [Online]. Available: https://doi.org/10.1038/s41598-017-07618-6

[4] M. Bahadori, M. Nikdast, S. Rumley, L. Y. Dai, N. Janosik, T. V. Vaerenbergh, A. Gazman, Q. Cheng, R. Polster, and K. Bergman, "Design space exploration of microring resonators in silicon photonicinterconnects: Impact of the ring curvature," *J. Lightwave Technol.*, vol. 36, no. 13, pp. 2767–2782, Jul 2018. [Online]. Available: http://jlt.osa.org/abstract.cfm?URI=jlt-36-13-2767

[5] M. Krause, "Finite-difference mode solver for curved waveguides with angled and curved dielectric interfaces," *IEEE/OSA Journal of Lightwave Technology - J LIGHTWAVE TECHNOL*, vol. 29, pp. 691–699, 03 2011.

[6] A. M. Hammond, "pymode," https://github.com/smartalecH/pyMode, 2019.

[7] F. Pedregosa, G. Varoquaux, A. Gramfort, V. Michel, B. Thirion, O. Grisel, M. Blondel, P. Prettenhofer, R. Weiss, V. Dubourg, J. Vanderplas, A. Passos, D. Cournapeau, M. Brucher, M. Perrot, and E. Duchesnay, "Scikit-learn: Machine learning in Python," *Journal of Machine Learning Research*, vol. 12, pp. 2825–2830, 2011.

[8] A. Oskooi, D. Roundy, M. Ibanescu, P. Bermel, J. Joannopoulos, and S. Johnson, "Meep: A flexible free-software package for electromagnetic simulations by the fdtd method," *Computer Physics Communications*, vol. 181, pp. 687–702, 03 2010.

[9] T. E. Oliphant, "Python for scientific computing," *Computing in Science Engineering*, vol. 9, no. 3, pp. 10–20, May 2007.

[10] S. G. Johnson, "The nlopt nonlinear-optimization package," http://github.com/stevengj/nlopt, 2017.

[11] M. Heuck, K. Jacobs, and D. R. Englund, "Photon-photon interactions in dynamically coupled cavities," *Physical Review A*, vol. 101, no. 4, Apr 2020.

[12] S. Ploeg, H. Gunther, and R. Camacho, "Simphony: An open-source photonic integrated circuit simulation framework," *Computing in Science Engineering*, pp. 1–1, 2020. [Online]. Available: https://ieeexplore.ieee.org/document/9149634

[13] S. Guha, "Structured optical receivers to attain superadditive capacity and the holevo limit," *Phys. Rev. Lett.*, vol. 106, pp. 1–4, Jun 2011. [Online]. Available: https://link.aps.org/doi/10.1103/PhysRevLett.106.240502

[14] A. M. Hammond, I. W. Frank, and R. M. Camacho, "Error correction in structured optical receivers," *IEEE Journal of Selected Topics in Quantum Electronics*, vol. 24, pp. 1–8, 2018.

[15] A. M. Hammond, E. Potokar, and R. M. Camacho, "Sip-ann," https://github.com/contagon/SiP-ANN, 2019.